Polymer 50 (2009) 4906–4916

Contents lists available at ScienceDirect

Polymer

journal homepage: www.elsevier.com/locate/polymer

Improving multifunctional behavior in structural electrolytes through copolymerization of structure- and conductivity-promoting monomers

James F. Snyder*, Eric D. Wetzel, Cara M. Watson

Materials Division, U.S. Army Research Laboratory, Aberdeen Proving Ground, MD 21005, USA

ARTICLE INFO

Article history:
Received 18 June 2009
Received in revised form
21 July 2009
Accepted 26 July 2009
Available online 8 August 2009

Keywords:
Electrolyte
Structural
Copolymer

ABSTRACT

Polymer electrolytes were developed to improve simultaneous demonstration of mechanical and electrochemical properties. Solvent-free random copolymers were synthesized using one monomer with poly(ethylene glycol) sidechains that promote lithium ion conduction and one crosslinking monomer that promotes high modulus. Sixty unique systems of monomer pairs were developed in this manner. The properties of the resulting copolymers were influenced by the monomer ratio and chemistry. The copolymers consistently exhibited improved electrochemical–mechanical multifunctionality with respect to the analogous homopolymers. The most promising systems included highly conductive components paired with highly structural components, suggesting that improved multifunctionality may be achieved through interpenetrating multicomponent systems in which each component demonstrates high efficiency in a single property. Electrochemical, mechanical, and viscoelastic properties are discussed with respect to composition and the glass transition temperature. Modeling of conductivity and modulus was employed to enable prediction of copolymer properties based on the ratio and properties of the constituents.

Published by Elsevier Ltd.

1. Introduction

The demand for advanced lightweight systems with increased capabilities has promoted research in multifunctional systems [1]. Multifunctional materials inherently possess two or more distinct, beneficial functionalities and can result in significant platform-wide weight savings as well as a wider range of available form factors. One example is multifunctional composites that can both store or produce energy while simultaneously bearing mechanical load [1–4]. These devices could potentially replace static load-bearing components in a traditional structure and provide auxiliary or remote power. If properly formulated, multifunctional composite devices may be processed into a wide variety of shapes and sizes.

To create a multifunctional energy-producing composite, such as a structural battery, one or more of the device constituents must possess load-bearing properties. Structural packaging has been considered previously and allows for the use of intact commercial battery devices and composites [2,5–7]. This approach is most effective for batteries in which packaging constitutes a significant fraction of battery weight, such as very thin or low-mass batteries. However, achieving weight savings using more massive batteries requires a different approach in which structural properties are designed directly into the electrolyte or electrode materials. The potential use of carbon fiber fabrics as structural anodes has been recently investigated with considerable promise [8]. Structural cathodes may be developed using thin-film technologies [9].

Designing a load-bearing electrolyte is more difficult since ion transport mechanisms typically conflict with desirable mechanical properties. In solvent-free polymer electrolytes, long-range ion conduction is enabled by local polymer motion [10]. Less mechanically robust polymers typically support higher conductivities. The addition of solvents, or the incorporation of state-of-the-art liquid electrolytes, can substantially degrade the mechanical properties of polymers. State-of-the-art liquid electrolytes have conductivities at 10^{-2} S/cm [11] while structural resins have stiffnesses that reach 4 GPa for thermosets and up to 8 GPa for highly oriented crystalline thermoplastics. Although these values are worthwhile targets for a structural electrolyte, lower values within a multifunctional system may still enable overall weight reduction though synergistic gains in conductivity, stiffness, and material dimensions.

Polymer-based electrolytes provide a convenient starting point for designing structural electrolytes due to their broad and tailorable mechanical properties and the ease with which resin monomers may be used in composites processing. The pursuit of solid-state polymer electrolytes has previously focused on flexible or rubbery

* Corresponding author. Tel.: +410 306 0842; fax: +410 306 0676.
E-mail address: jsnyder@arl.army.mil (J.F. Snyder).

0032-3861/$ – see front matter Published by Elsevier Ltd.
doi:10.1016/j.polymer.2009.07.050

systems that may be useful as the separator in conformal and thin film batteries. Approaches for improving the stiffness of polymer electrolytes have included crosslinking [12,13], small particle fillers [14–17], and block copolymers [18–20]. However, these approaches have been unable to demonstrate superior mechanical properties while maintaining sufficient ion conductivity. These investigations are also frequently limited to narrow compositional ranges to maintain high conductivities, so the broad spectrum of electrochemical–mechanical properties remains largely ill-defined, particularly regarding high-modulus systems.

The present study extends previous work investigating the potential use of poly(ethylene glycol) (PEG) based vinyl ester polymer electrolytes for multifunctional structural applications [21]. Vinyl ester resins offer the benefit of a wide range of functional groups, architectures, and variable degrees of networking with which to effectively present a broad study of electrochemical–mechanical multifunctionality in polymer systems. Vinyl ester-based electrolytes have been previously investigated for their dimensional stability [22] but they typically serve only as reinforcement in polymer gels [23,24]. In the current study these systems have been prepared without the addition of secondary solvents, since the PEG etheric oxygen groups in the monomers are capable of dissociating the donor salt ions. The absence of solvents simplifies the analyses of electrochemical–mechanical properties as a function of polymer chemistry and architecture. Radical polymerization, or addition reaction of a second species to the vinyl group, may be employed to achieve a solid electrolyte. Conductivity in the absence of solvent is enabled by short-range hopping between occupation sites coupled with mobility of the polymers. Structural properties are provided by the vinyl ester networks.

It was found in our previous work that vinyl ester homopolymers with a wide variety of chemical functionalities and architectures yielded similar tradeoffs in ion transport and mechanical robustness, such that no particular advantages in electrochemical–mechanical multifunctionality were achievable through homopolymer design [21]. One problem with these materials is that in solvent-free polymer electrolytes, ion transport relies on segmental mobility of the polyethylene glycol (PEG). Crosslinking these vinyl ester resins results in binding both ends of the PEG chains, thereby significantly reducing the potential mobility of the PEG. The materials that demonstrated the highest ion conductivity were comb polymers with PEG oligomer sidechains that retain some mobility. The materials that demonstrated the highest mechanical stiffness were crosslinked, preventing substantial ion transport. Similarly, Torquato et al. have postulated that it is difficult to develop homogenous materials that exhibit multiple high performance characteristics, and that materials with multiple constituents are more suitable to achieve multifunctionality by combining the best features of different materials [25].

In the study reported here, random copolymers were formulated that include both comb and crosslinking segments. In this way a structural scaffold is generated through crosslinking while PEG sidechains enhance ion transport. The same monomers that were investigated in our previous work are also used in this study to compare homopolymer and copolymer systems across a broader range of chemistries and architectures.

2. Experimental

2.1. Materials

Fig. 1 depicts the nomenclature and generic structural representations for the materials employed in this study. The monomers are vinyl ester derivatives of PEG and follow the same nomenclature as described in our initial work with homopolymers, *mXn-Y* [21]. The variable *m* represents the number of polymerizable vinyl ester groups, *X* represents the type of vinyl ester, *n* represents the total number of oligoether units, and *Y* represents an additional functional group that may be at the terminal end of a mono-vinyl ester, or that may bisect the PEG units in the other monomers. The copolymers are derived from combining "comb" monomers containing a single vinyl ester group (*mXn-Y*, $m = 1$) with "crosslinker" monomers containing 2-4 vinyl ester groups (*mXn-Y*, $m > 1$). Within the scope of this study, the first term ($m_1X_1n_1-Y_1$) will always refer to a comb-type monomer and the second term will always refer to a crosslinking monomer. Fig. 1b graphically depicts representative architectures that may be formed through the copolymerization of these monomers.

The monomers were supplied by Sartomer Company (Exton, PA), with the following product codes: methoxy-terminated monovinyl monomers: CD550, CD552, CD553; hydroxyl-terminated monovinyl monomers: CD572; divinyl PEG monomers: SR209, SR252, SR259, SR610, SR344, SR480; divinyl PEG monomers bisected with a bisphenol-A functional group: SR601, SR602, SR603, SR9036, CD9038; trivinyl monomers: SR454, SR502, SR9035; and tetravinyl monomer: SR494. With the exception of CD570, all of the monomers are at least 98% of the labeled component according to the MSDS sheets supplied by Sartomer. CD570 is a mixture of two similar compounds that differ only by the length of the PEG oligomer, the minor component comprising 21% of the solution. The monomers were stored between uses in a refrigerator in brown glass bottles under nitrogen atmosphere and sealed with Parafilm. Unless otherwise noted all reagents were used as received and handled exclusively in a glovebox under dry nitrogen, or in an oven with a continuous nitrogen purge. Care was taken to handle the polymerized materials exclusively under dry nitrogen or dry air, with the exception of compression testing, which occurred under ambient atmosphere.

Lithium triflate (Aldrich) was used exclusively as the lithium salt to prepare monomer and polymer complexes. Lithium triflate provides high thermal and chemical stability while maintaining low toxicity, low cost, and a significant presence in the research literature upon which comparisons with other materials may be made.

2.2. Polymer preparation

Monomer-salt complexes were prepared according to the procedure described earlier [21]. A fixed concentration of 12% lithium triflate w/w PEG was used. This concentration of salt provides a 30:1 ratio of etheric oxygen groups to lithium ions and was found to be a generally favorable concentration with respect to multifunctional attributes for these materials as homopolymers [21]. Monomer-salt complexes were then added to 4 mL glass vials according to the desired formulation and mixed thoroughly. The resulting solutions were poured into rubber molds and polymerized under dry nitrogen at 80 °C for at least 8 h followed by one hour at 100 °C. The samples were then allowed to cool to room temperature. Pellets ca. 12 mm diameter and 3 mm thick were fabricated for impedance spectroscopy and compression and were prepared for all samples in the matrix. Prismatic bars ca. 60 mm long, 12 mm wide and 4 mm thick, were fabricated for dynamic mechanical analyses and were only prepared for downselected monomer combinations.

2.3. Electrochemical Impedance Spectroscopy (EIS)

EIS was conducted using a Solartron 1260 Impedance/Gain-Phase Analyzer and Solartron 1287 Electrochemical Interface across a frequency range of 10^6 Hz–10 Hz at room temperature (18–20 °C). Each sample was assembled under a dry air atmosphere (<5 ppm water) between stainless steel blocking electrodes in a test cell. Bulk resistance, *R*, was acquired using ZPlot software by fitting the

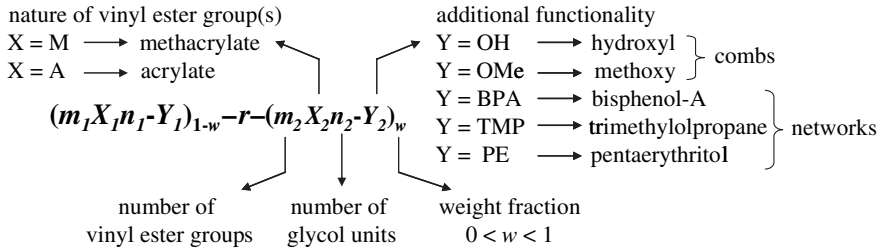

a

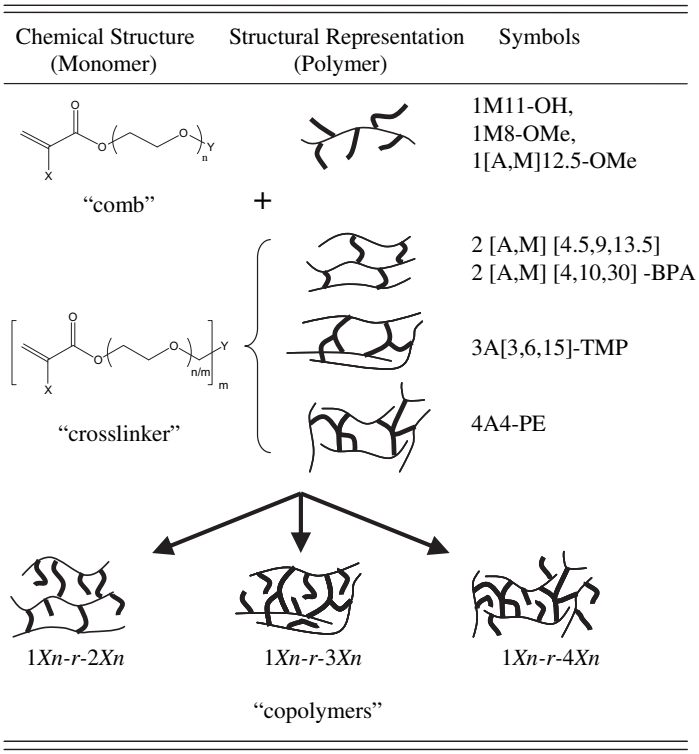

b

Fig. 1. (a) A formulaic representation of copolymers PEG vinyl ester derivatives. (b) Generic chemical structures of the monomers employed in this study and representative examples of their polymerized structures as both homopolymers and copolymers. The "symbols" column describes the complete set of monomers employed in this study. Square brackets contain multiple variations such that 2[A,M][4.5,9,13.5] represents a set of six monomers, 3 diacrylates with PEG oligomers containing 4.5, 9, or 13.5 units on average; and 3 dimethacrylates of similar composition. Bold lines in the cartoons represent PEG regions while thin lines represent polyacrylic regions. 50:50 monomer ratios, ABAB polymer structure, and full conversion are assumed in the cartoons for purposes of demonstrating the variable impact of branching.

impedance data to an equivalent circuit. Resistance was converted to conductivity, σ, using equation (1):

$$\sigma = \frac{l}{R \times A} \tag{1}$$

where l is the path length (pellet thickness) and A is the cross-sectional area of the path calculated from the pellet diameter. Over all of the material systems investigated, the average margin of error for conductivity as calculated from the standard deviation of two or more pellets was 12%, with a median of 6%. These errors are attributed to uneven sample dimensions and to cracks and defects that may have formed during handling.

2.4. Compression testing

Compression testing was conducted at room temperature under ambient atmosphere using an MTS Synergie load frame with a 5-kN load cell. The method was adapted from ASTM D695-02a. Each experiment lasted for approximately 2 min. The tests were run in a displacement control mode at a cross-head speed of 1 mm/min. System compliance introduced error into the displacement and strain measurements due to the low aspect ratio of the samples. The instrument was therefore evaluated each day of testing by recording displacement when no sample was placed between the cross-heads. This load-displacement curve was then used to normalize the property measurements. Due to the large strains induced during the tests, the compressive stiffness, E_c, for each sample was calculated from the true stress and true strain values. The average margin of error as calculated from the standard deviation of two or more pellets was 14%, with a median of 10%. The origins and impact of compression error are similar to that described above for impedance error.

2.5. Dynamic Mechanical Analysis (DMA)

DMA was conducted at a single frequency across a temperature sweep using a Thermal Advantage DMA Q800 and associated

software. Each prismatic bar was clamped into the three-point sample holder and hand-tightened at room temperature. The chamber temperature was then reduced to −130 °C and the clamps were retightened to 0.5 MPa using a torque wrench. Lightly crosslinked polymers were manually retightened to a lesser pressure of approximately 0.1 MPa to prevent cracking. The chamber temperature was then reduced to −135 °C and held at constant temperature for 1 min. Data was collected for thermal transition from −135 °C to 150 °C at 2 °C/min. Higher glass transition samples were heated to 250 °C. Samples were tested at 1 Hz using a 7.5 μm amplitude.

The DMA measurements yielded the temperature dependence of storage moduli (E'), loss moduli (E'') and loss tangent (tan δ). The E' at 20 °C, E' at the rubbery plateau ($E'_{\min}$), E'' peak maximum, tan δ peak maximum, and tan δ full width at half maximum (FWHM) were recorded. T_g was determined from the temperature corresponding to the E'' peak maximum. The average molecular weight between cross-links, M_c, was calculated according to the theory of Rubber Elasticity using equation (2) [26,27]:

$$E'_r = \frac{3RT\rho}{M_c} \tag{2}$$

in which E'_r is the storage modulus in the rubbery region (taken to be $E'_{\min}$) at a given temperature (T) and polymer density (ρ). Calculations for M_c do not yield reliable absolute numbers, but the relative trends among similar materials can yield a better understanding of the material behavior.

2.6. Fourier-Transform Infrared Spectroscopy (FT-IR)

Experiments to monitor extent of cure were conducted on a Thermo Nicolet Nexus 870 using samples formed into pellets. Liquid monomers, without salt, of the desired compositions were measured for reference. The conversion, α, at time t was determined from the absorption peak heights, β, for a peak directly impacted by the reaction and a reference peak that is not affected by the reaction, as shown in Equation (3) [28]:

$$\alpha(t) = 1 - \left(\frac{\beta(t)_{\text{peak}}}{\beta(t=0)_{\text{peak}}}\right) \times \left(\frac{\beta(t=0)_{\text{reference}}}{\beta(t)_{\text{reference}}}\right) \tag{3}$$

OMNIC 6.0 software was used to monitor the vinyl stretching mode peak in the near-IR region of the spectrum at 6160 cm^{-1} and a reference peak at 5790 cm^{-1}.

3. Results

3.1. Polymer properties

Table 1 summarizes characterization data measured for several sample sets representing a variety of architectures. The near-IR conversion experiments indicated conversion is near 100% for all samples. These high conversions suggest that variations between samples in this study do not appear to result from variations in extent of cure. The slightly reduced conversions in highly crosslinked samples result from the formation of infinite networks that prematurely arrest system mobility [29,30]. Increasing the concentration of comb-type monomers improves conversion efficiencies because the combs act as chain extenders that increase the distance between crosslinks and delay the formation of infinite networks. High conversion is generally desired to reduce the number of unreacted functional groups remaining in the sample. Unreacted functionalities could provide undesirable chemical or thermal instability in an operating electrochemical device.

The material properties in Table 1 generally indicate a smooth transition as the compositions change from more compliant, linear polymers to rigid, highly networked polymers. The storage and loss moduli are depicted in Fig. 2 for the (**1A12.5-OMe**)$_{1-w}$-*r*-(**4A4-PE**)$_w$ series. Reduced temperature ($T - T_g$) is used on the x-axis to facilitate comparison. The storage moduli in the rubbery region increase with increased crosslinking according to expectations. The storage moduli at 20 °C approximates room temperature behavior and shows similar trends as compressive moduli, although specific values differ due to the test methods.

The values of the loss moduli peaks decrease with increased crosslinking, demonstrating approximately linear behavior with change in composition. This trend indicates decreasing viscous behavior in the material that may result from less energy dissipation as the mobility of the polymer backbone is reduced, as well as the loss of mobile sidechains as less comb-type monomer is introduced. $E''_{\max}$ and related tan $\delta_{\max}$ appear to be abnormally low for **1A12.5-OMe** resulting in deviation from the evident trend for each series. However, **1M12.5-OMe** does not demonstrate this deviation as shown in both Table 1 and Fig. 2, as it has significantly larger viscosity-related values in spite of being nearly identical to **1A12.5-OMe**. This anomaly may be attributed to DMA measurement errors for **1A12.5-OMe** due to its tackiness and lack of dimensional stability at room temperature. The sample was necessarily pre-frozen in order to load it in the instrument, which may have introduced various errors. The misshapen transition region unfortunately occurred in each of several retrials. Much of the remaining information (e.g. transition onset) appears to have been relatively unaffected and was repeatable, within expectation, and similar to the values derived from **1M12.5-OMe**.

The T_g increases with increasing mass fraction of crosslinker for each sample set, as illustrated in Fig. 3. Secondary transitions were not readily apparent in the DMA spectra, indicating that there is no phase separation in the copolymer systems. Phase separation was not anticipated since the monomers in each system were miscible prior to co-polymerization. In addition, all of the monomers include at least one oxyethylene unit adjacent to the vinyl ester group, which should minimize differences in reactivity ratios between monomers and promote their distribution within the cured polymer. Although a large difference in reactivity ratios between acrylates and methacrylates is still anticipated for systems that mix these two functional groups [31], any resultant clustering of a single monomer type did not result in a substantial difference in properties relative to acrylate-only or methacrylate-only systems.

The width of transition between the glassy and rubbery regions, gauged quantitatively in Table 1 using the full width at half maximum (FWHM) of the loss tangent peak, initially increases with increased crosslinking. This trend is compatible with previous observations that the FWHM increases with increased crosslink density for the homopolymers, which may be attributed to the greater variance in localized mobility as crosslinks are formed [21]. The formation of microgels may also serve to broaden the transition, an effect that has been observed among crosslinked PEG dimethacrylates as the crosslink length is reduced [32]. The subsequent decrease in FWHM for several of the crosslinked homopolymers may reflect the absence of low T_g comb sidechains, which bring some measure of heterogeneity to the copolymer systems. The anomalous system, (**1A12.5-OMe**)$_{1-w}$-*r*-(**2A30-BPA**)$_w$, has very long crosslinks and exhibits little to no variation in tan $\delta_{\max}$ with crosslink density.

Fig. 4 illustrates the conductivities (Fig. 4a) and compressive moduli (Fig. 4b) for 15 systems, including those from Table 1, in which a single comb-generating monomer (**1A12.5-OMe**) has been polymerized with a wide variety of crosslink-generating monomers in relative mass ratios of 1:2, 1:1, and 2:1. The homopolymer endpoints are also included. A logarithmic axis is used for each

Table 1
Properties of several solvent-free random copolymer electrolytes described in Fig. 1.[a]

Resin Description	Type	Conversion (FTIR)	σ (S/cm)	T_g (°C)	E_c (MPa) ~ 20°C	E' (MPa) 20 °C	E'' (MPa) peak max.	tan δ		M_c (g) MW_{XL}
								Peak max.	Peak width	
1A12.5-OMe	Uncrosslinked Hompolymer	100%	3.5E-05	−48 (−41)[b]	0.4	0.2 (0.5)[b]	297 (537)[b]	0.46 (2.27)[b]	12 (17)[b]	–
(1A12.5-OMe)$_{0.75}$-*r*-(4A4-PE)$_{0.25}$	Copolymer	100%	4.0E-06	−39	26	9	423	0.53	36	1689
(1A12.5-OMe)$_{0.5}$-*r*-(4A4-PE)$_{0.5}$	Copolymer	98%	5.9E-07	−30	99	122	306	0.21	98	259
(1A12.5-OMe)$_{0.25}$-*r*-(4A4-PE)$_{0.75}$	Copolymer	97%	5.5E-08	−14	712	901	176	0.13	109	67
4A4-PE	Crosslinked Hompolymer	89%	5.9E-09	20	784	1758	120	0.18	84	57
1A12.5-OMe	Uncrosslinked Hompolymer	100%	3.5E-05	−48 (−41)[b]	0.4	0.2 (0.5)[b]	297 (537)[b]	0.46 (2.27)[b]	12 (17)[b]	–
(1A12.5-OMe)$_{0.75}$-*r*-(3A3-TMP)$_{0.25}$	Copolymer	100%	3.4E-06	−39	17	5	380	0.66	32	3078
(1A12.5-OMe)$_{0.5}$-*r*-(3A3-MTP)$_{0.5}$	Copolymer	100%	5.5E-07	−30	89	93	306	0.24	92	369
(1A12.5-OMe)$_{0.25}$-*r*-(3A3-TMP)$_{0.75}$	Copolymer	98%	1.1E-07	−13	407	810	168	0.18	99	49
3A3-TMP	Crosslinked Hompolymer	90%	1.6E-08	4	562	1113	149	0.27	80	70
1A12.5-OMe	Uncrosslinked Hompolymer	100%	3.5E-05	−48 (−41)[b]	0.4	0.2 (0.5)[b]	297 (537)[b]	0.46 (2.27)[b]	12 (17)[b]	–
(1A12.5-OMe)$_{0.75}$-*r*-(2M4.5)$_{0.25}$	Copolymer	100%	3.8E-06	−41	8	2	443	0.78	31	6445
(1A12.5-OMe)$_{0.5}$-*r*-(2M4.5)$_{0.5}$	Copolymer	100%	6.1E-07	−31	72	48	296	0.30	83	657
(1A12.5-OMe)$_{0.25}$-*r*-(2M4.5)$_{0.75}$	Copolymer	99%	5.3E-08	−12	417	742	168	0.24	61	355
2M4.5	Crosslinked Hompolymer	96%	1.3E-08	71	2055	2138	162	0.37	57	157
1A12.5-OMe	Uncrosslinked Hompolymer	100%	3.5E-05	−48 (−41)[b]	0.4	0.2 (0.5)[b]	297 (537)[b]	0.46 (2.27)[b]	12 (17)[b]	–
(1A12.5-OMe)$_{0.75}$-*r*-(2A4.5)$_{0.25}$	Copolymer	100%	3.6E-06	−38	11	3	386	1.11	19	5644
(1A12.5-OMe)$_{0.5}$-*r*-(2A4.5)$_{0.5}$	Copolymer	100%	6.6E-07	−25	36	17	308	0.52	28	866
(1A12.5-OMe)$_{0.25}$-*r*-(2A4.5)$_{0.75}$	Copolymer	100%	8.6E-08	−3	112	45	184	0.51	27	758
2A4.5	Crosslinked Hompolymer	99%	1.6E-08	40	162	1480	185	0.47	26	237
1A12.5-OMe	Uncrosslinked Hompolymer	100%	3.5E-05	−48 (−41)[b]	0.4	0.2 (0.5)[b]	297 (537)[b]	0.46 (2.27)[b]	12 (17)[b]	–
(1A12.5-OMe)$_{0.75}$-*r*-(2A4-BPA)$_{0.25}$	Copolymer	100%	3.2E-06	−35	13	3	398	1.06	20	4773
(1A12.5-OMe)$_{0.5}$-*r*-(2A4-BPA)$_{0.5}$	Copolymer	99%	3.8E-07	−22	59	11	271	0.57	33	867
(1A12.5-OMe)$_{0.25}$-*r*-(2A4-BPA)$_{0.75}$	Copolymer	100%	6.0E-08	2	336	229	125	0.48	37	897
2A4-BPA	Crosslinked Hompolymer	80%	7.0E-09	26	694	1499	236	0.49	37	1354
1A12.5-OMe	Uncrosslinked Hompolymer	100%	3.5E-05	−48 (−41)[b]	0.4	0.2 (0.5)[b]	297 (537)[b]	0.46 (2.27)[b]	12 (17)[b]	–
(1A12.5-OMe)$_{0.75}$-*r*-(2A30-BPA)$_{0.25}$	Copolymer	100%	1.4E-05	−41	4	2	511	2.24	11	14628
(1A12.5-OMe)$_{0.5}$-*r*-(2A30-BPA)$_{0.5}$	Copolymer	100%	5.4E-06	−36	8	3	412	1.86	11	4794
(1A12.5-OMe)$_{0.25}$-*r*-(2A30-BPA)$_{0.75}$	Copolymer	100%	2.6E-06	−30	13	2	289	1.65	10	3567
2A30-BPA	Crosslinked Hompolymer	99%	1.7E-06	−23	15	5	370	1.55	9	4714

[a] The resins described in Fig. 1 are complexed with lithium triflate at 12% w/w weight fraction PEG in each monomer. The chart includes conversion as determined by FT-IR, ion conductivity (σ), glass transition temperature (T_g), compressive stiffness (E_c), storage modulus (E'), loss modulus (E''), loss tangent (tan δ), and the average molecular weight between cross-links (M_c).

[b] The values in parenthesis were measured for **1M12.5-OMe**, a very similar polymer to **1A12.5-OMe** that yielded more reliable viscoelastic data due to the relative lack of dimensional stability of **1A12.5-OMe** at room temperature and the resulting difficulty with loading the sample on the DMA instrument.

property to adequately display the range of values. These 15 systems were repeated using three other comb-generating monomers (**1M12.5-OMe**, **1M8-OMe**, **1M-11-OH**) and produced similar results. The log conductivity typically demonstrated linear behavior with respect to the monomer ratio, which is demonstrated by the evenly spaced curves in Fig. 4a. In contrast, log modulus does not demonstrate simple linear behavior. Instead, the initial crosslinks have the greatest relative impact on log modulus such that 50% of the difference between the endpoints is achieved between 0% and 25% crosslinker. The last increment, which is from 75% to 100% crosslinker, accounts for only 10% of the overall change in log modulus.

3.2. Multifunctional behavior

The multifunctional behavior of the structural electrolytes described here is best understood through the interdependence of ion conductivity, representative of the desired electrochemical behavior; and polymer modulus, representative of the desired mechanical behavior. Fig. 5 illustrates the variations of ion conductivity as a function of compressive modulus for all of the materials in the current study. Samples with better multifunctionality will exhibit higher combined conductivity and modulus values. Homopolymer data corresponding to each monomer in this study is illustrated in Fig. 5a and shows overall simple log-log dependence of the properties that has been explained in detail elsewhere [21]. A linear fit of the homopolymer samples on these log-log coordinates outlines the overall homopolymer trend to provide a baseline for more straightforward comparison in the other figures. The slope of the fit is 1.17, which suggests that the tradeoff between conductivity and modulus is close to 1:1 on these logarithmic axes as the chemistry and architecture are varied among homopolymers.

Fig. 5b–d illustrate data pertaining to copolymer samples. Fig. 5b exhibits the full matrix of copolymers described by Fig. 4. The majority of this data show enhanced multifunctional behavior relative to the baseline, represented by the linear fit to the homopolymers from Fig. 5a. The greatest enhancement was evident with the (**1A12.5-OMe**)$_{1-w}$-*r*-(**4A4-PE**)$_w$ series, which combines a crosslinker that has the greatest degree of branching and one of the highest moduli in this study with a comb that has the highest conductivity in this study.

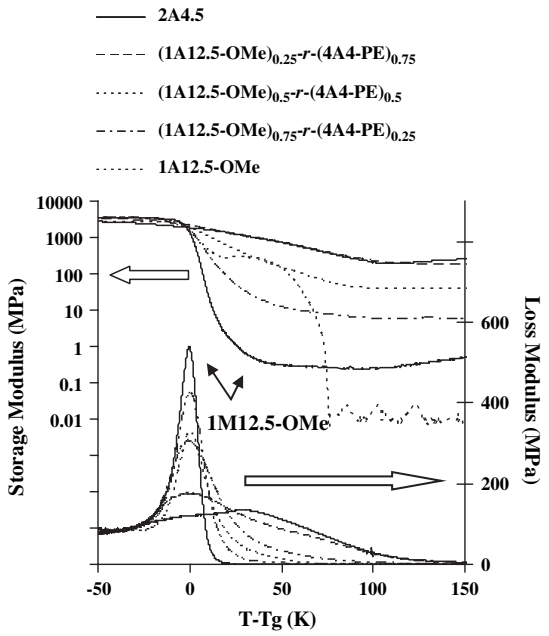

Fig. 2. Storage and loss moduli for the $(\mathbf{1A12.5\text{-}OMe})_{1-w}$-*r*-$(\mathbf{4A4\text{-}PE})_w$ series of copolymers plotted against reduced temperature ($T - T_g$).

Fig. 5c isolates the impact of using a high modulus crosslinker, **4A4-PE**, with select combs of differing functionality and sidechain length. Fig. 5d isolates the impact of using a high conductivity comb, **1A12.5-OMe**, with select crosslinkers of differing functionality and degree of networking. The evident trends are for the data to follow a convex path between homopolymer endpoints, with maximum positive deviation from homopolymer behavior for samples with mixed comb-crosslinker composition. Each of the 60 individual sample sets embedded in Fig. 5b follows this behavior.

4. Discussion

4.1. Polymer properties

The conductivity data in Fig. 4a suggests that formulation-dependent changes in crosslinking and availability of ionic pathways have a logarithmic impact on ion transport behavior. A similar relationship between conductivity and composition has been described previously for polymer electrolytes plasticized with liquid [33]. An exponential equation used to empirically model that data also fits the current data quite accurately, as shown in Fig. 6, and is described by:

$$\sigma = Ce^{-Dw} \tag{4}$$

in which w is the weight percent crosslinking polymer, and C and D are fitting parameters. For the current study, $\sigma = \sigma_{comb} = C$ at $w = 0$, and $\sigma = \sigma_{crosslinker} = C \times e^{-D}$ at $w = 1$. Using these endpoints, the fitting parameters may therefore be set to $C = \sigma_{comb}$ and $D = \ln(\sigma_{comb}/\sigma_{crosslinker})$ for any given system and equation (4) may be rewritten as:

$$\sigma = (\sigma_{comb})^{1-w}(\sigma_{crosslinker})^{w} \tag{5}$$

Equation (5) may be useful for predicting the conductivities of other copolymer systems based on the relative mass fractions of the constituents and their homopolymer conductivities. It may also be applicable to other mixed systems, such as polymers plasticized with liquid electrolytes, especially considering that equation (4) originated with plasticized systems. It should be noted that equation (5) is limited to constant temperature conditions.

Effective prediction of conductivities in multicomponent systems may be extended to include temperature dependence by combining equation (5) with the empirical Vogel-Tamman-Fulcher (VTF) or Arrhenius equations. These equations are frequently used to describe the temperature dependence of ion conductivity in polymer electrolytes above and below T_g, respectively. Since most useful electrolytes are above T_g at operating temperature, the focus here will only be on the VTF equation:

$$\sigma T^{1/2} = Ae^{-\frac{B}{k(T-T_0)}} \tag{6}$$

where A is a pre-factor that is often related to the number and mobility of charge carriers, B is a pseudo-activation energy, k is the Boltzmann constant, and T_0 is the ideal glass transition temperature typically found to be about 40 K below the measured T_g [34]. For an amorphous polymer electrolyte, $\log\sigma$ vs. $(T-T_0)^{-1}$ is typically linear, with a slope proportional to B per the VTF equation. Below T_0 the conductivity typically adheres to Arrhenius behavior, exhibiting a logarithmic dependence with respect to T^{-1}. Defining σ_{comb} and $\sigma_{crosslinker}$ by equation (6), and substituting into equation (5), yields:

$$\sigma = T^{-1/2}\left(A_{comb}e^{-\frac{B_{comb}}{k(T-T_{0\ comb})}}\right)^{1-w} \times \left(A_{crosslinker}e^{-\frac{B_{crosslinker}}{k(T-T_{0\ crosslinker})}}\right)^{w} \tag{7}$$

A similar equation, or combinations thereof, may be derived using the Arrhenius equation. According to equation (7), once the VTF parameters are known for two homopolymer electrolytes, the conductivity of all random copolymer derivatives may be predicted for any temperature, i.e. the data set $\sigma(w,T)$. Given sufficient homogeneity, equations (5) and (7) may also apply to polymer blends and gels.

It is noteworthy that equations (4) and (6) have a similar form. The governing relationship between these two equations concerns the impact of $T-T_g$ on conductivity. The VTF equation relates conductivity to changes in temperature for a single material with

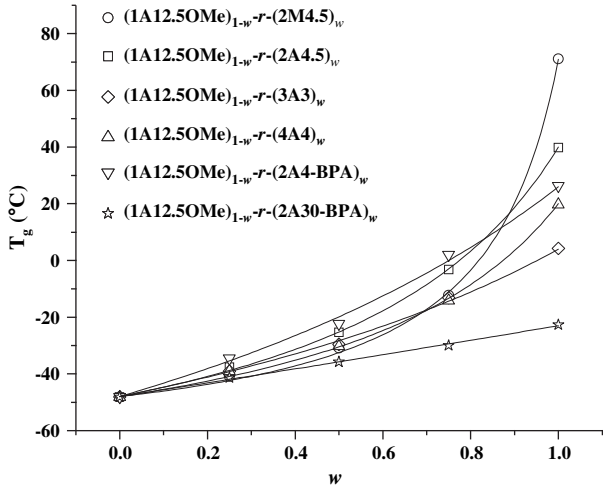

Fig. 3. Glass transition temperatures as a function of polymer composition for the samples in Table 1. The samples are fit using the Gordon–Taylor equation (equation (8)).

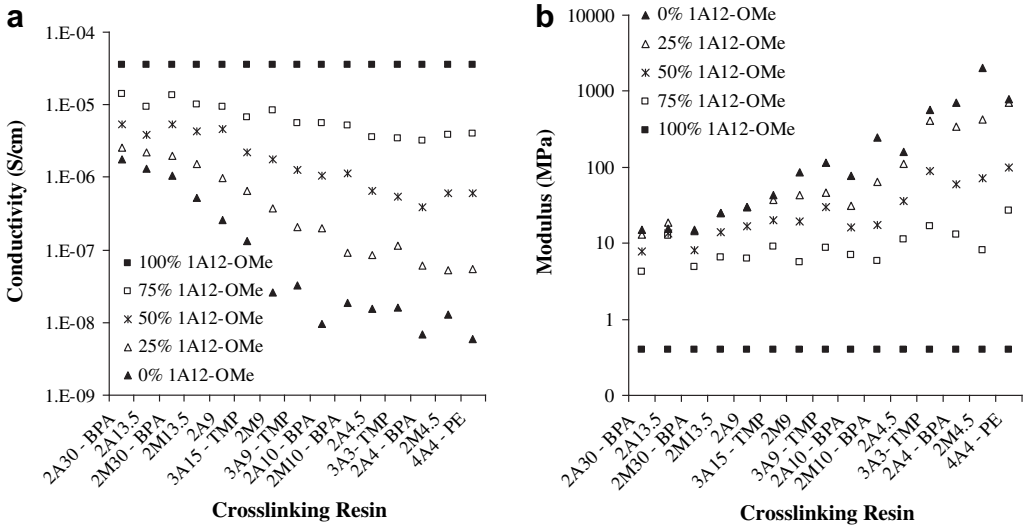

Fig. 4. The impact of changing the ratio of monomer components on (a) ion conductivity and (b) compressive modulus at room temperature for samples listed in Fig. 1 in which a highly conductive comb monomer has been combined with each of the crosslinking monomers investigated in this study.

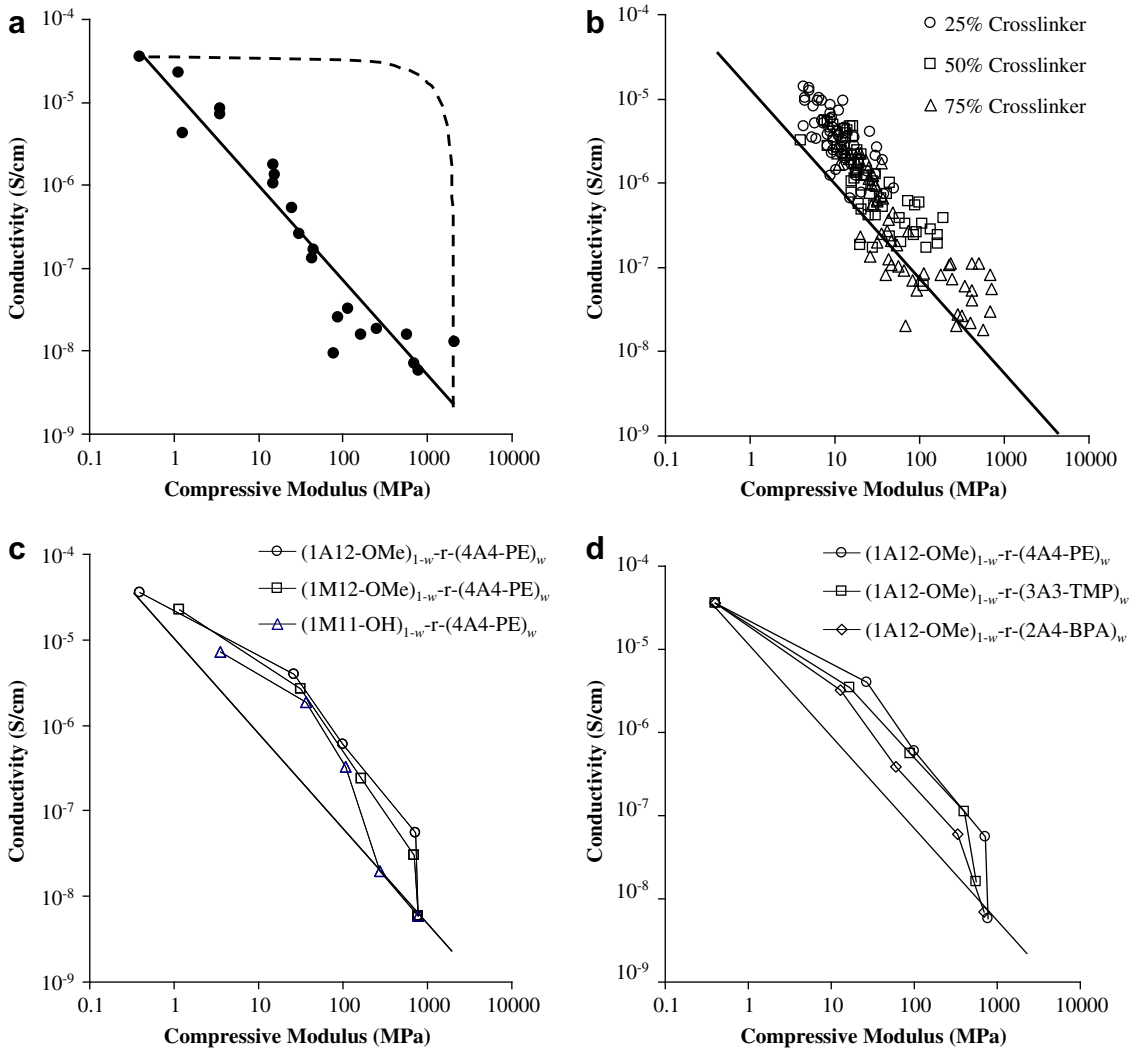

Fig. 5. Conductivity vs. compressive modulus for the samples listed in Fig. 1 at room temperature. (a) Homopolymer samples, (b) copolymer samples, (c) samples that result from combining each of several conductive comb monomers with a crosslinking monomer that yields high stiffness, and (d) samples that result from combining each of several structural crosslinking monomers with a comb monomer that yields materials with relatively high ion conductivity. A linear fit (on these log-log axes) for the homopolymer data are shown in all four graphs. The dashed line in (a) is a linear fit for the endpoints, shown to contrast log–log behavior to linear behavior.

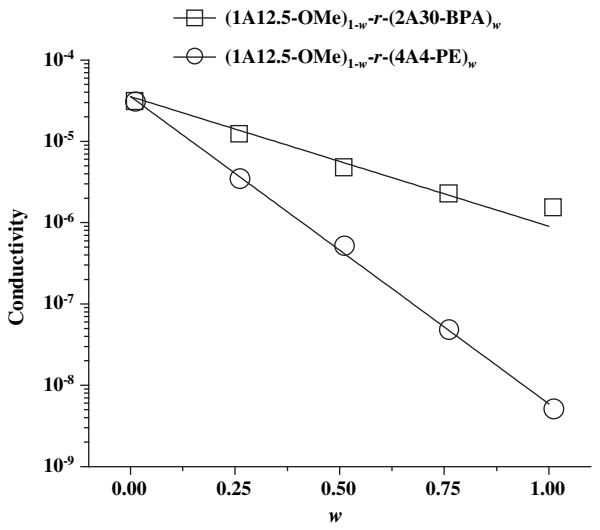

Fig. 6. Conductivity vs. composition at room temperature for two disparate sample sets that have been fit using equation (5).

a single T_g. Equation (4) relates conductivity to changes in T_g via changes in composition and architecture for a single temperature.

Identification of mixing rules for modeling copolymer mechanical behavior is less straightforward. Fig. 7a and b show compressive modulus as a function of crosslinking monomer mass fraction for the (**1A12.5-OMe**)$_{1-w}$-*r*-(**2A30-BPA**)$_w$ and (**1A12.5-OMe**)$_{1-w}$-*r*-(**2M4.5**)$_w$ series, respectively. While the latter system is a mixed acrylate/methacrylate copolymer that may not be truly random in monomer distribution due to the difference in reactivity ratios [31], behavior similar to Fig. 7b was also noted for all-acrylate copolymers with other rigid crosslinkers. The two crosslinking monomers chosen for comparison in Fig. 7 represent the least stiff (**2A30-BPA**) and most stiff (**2M4.5**) crosslinking homopolymers in this study. The ratio of crosslinking homopolymer modulus to comb homopolymer modulus for the **2A30-BPA** and **2M4.5** cases is ca. 40 and ca. 5000, respectively. For the low stiffness ratio case (Fig. 7a), compressive modulus increases linearly with crosslink monomer mass fraction. For the high stiffness ratio case (Fig. 7b), modulus increases very little at low crosslink monomer content, then increases rapidly between 50 and 100% mass fraction.

Also shown in Fig. 7a and b are theoretical mixing models for mechanical stiffness. These models generally use phase volume fraction and pure phase elastic properties to predict composite stiffness values. Isostrain (Voigt), isostress (Reuss), and Hashin-Strikman (HS) bounds represent theoretical extremes in mixed behavior [35]. The HS bounds in primitive form determine bulk and shear moduli, so Young's modulus was calculated by assuming a Poisson's ratio of 0.4 [36]. Also shown are two models that have been applied to co-continuous architectures: the two-phase interpenetrating composite model of Feng et al. [37] and the effective medium approximation (EMA) for the case of spherical inclusions [38]. A Poisson's ratio of 0.4 was also used for the EMA model. For all models, homopolymer densities are assumed to be equal so that volume fraction is equivalent to mass fraction. For the low stiffness-ratio case (**2A30-BPA**), the copolymer modulus is well-modeled by a simple isostress model. In contrast, the high stiffness-ratio case (**2M4.5**) shows behavior that is more closely modeled by the co-continuous material models. Similar plots of compressive modulus versus crosslinking monomer volume fraction for all crosslinking monomers characterized in this study (not shown) show a steady transition from linear behavior towards non-linear behavior as the stiffness ratio of the homopolymers increases. In most cases, the data tends to most closely follow the co-continuous Feng and EMA models. These results suggest that the copolymer is adopting a well-mixed, interpenetrating network of phases that largely maintain their homopolymer character. These behaviors also show that, for cases of high crosslink-to-comb stiffness ratio, higher volume fractions of crosslinking monomer are necessary to achieve the levels of geometric percolation sufficient for robust mechanical properties.

The dependence of conductivity and moduli on composition can also be analyzed in terms of $T - T_g$, as shown in Fig. 8. Two of the copolymer systems illustrated earlier (Fig. 5d) are shown alongside data corresponding to all of the homopolymers. The conductivity behavior as a function of $T - T_g$ is similar for homopolymers and copolymers, indicating that $T - T_g$ is an effective measure of polymer mobility as it relates to ionic conductivity. However, the copolymers generally show higher mechanical properties than homopolymers at an equivalent $T - T_g$. The result suggests that the improved multifunctional character of the copolymer systems is enabled by partially decoupling bulk mechanical properties from the polymer mobility as measured by $T - T_g$. This decoupling may be enabled by the formation of interpenetrating networks, at either

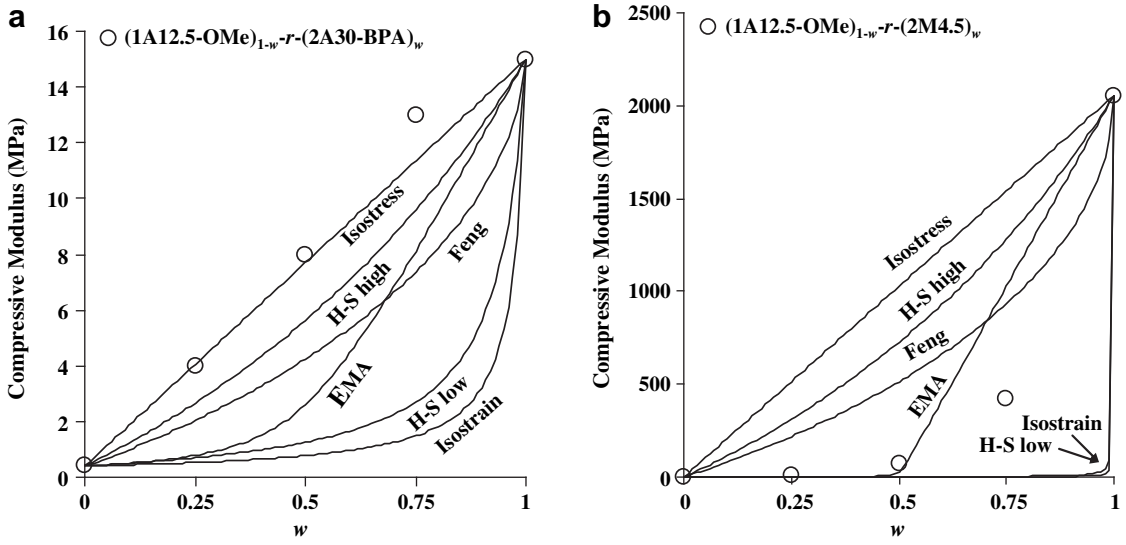

Fig. 7. Experimental and model predictions for room temperature compressive modulus as a function of crosslink monomer mass fraction w for the copolymer series (a) (**1A12.5-OMe**)$_{1-w}$-r-(**2A30-BPA**)$_w$ and (b) (**1A12.5-OMe**)$_{1-w}$-r-(**2M4.5**)$_w$.

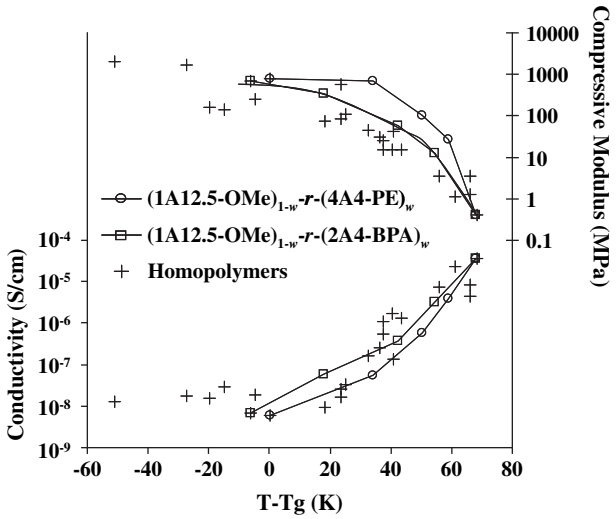

Fig. 8. Conductivity and modulus vs. $(T-T_g)^{-1}$ for several sample sets.

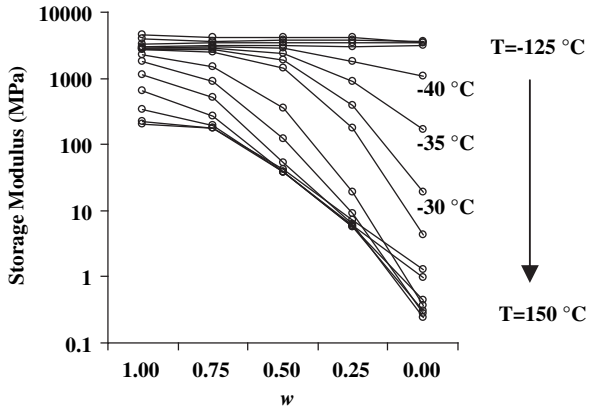

Fig. 9. Storage modulus vs. composition for the $(\mathbf{1A12.5\text{-}OMe})_{1-w}$-**r**-$(\mathbf{4A4\text{-}PE})_w$ series of copolymers at measurement temperatures in 25°C increments between −125 °C and 150 °C. Three additional temperature curves within the transition region are shown for clarity and are explicitly marked. The data was extracted from the curves shown in Fig. 2. **1M12.5-OMe** was used as the comb endpoint to account for the anomalies with **1M12.5-OMe** evident in Fig. 2.

a molecular or super-molecular scale, of structure (crosslinks) and ion transport (sidechains).

Compression experiments over a broader range of $T-T_g$ than shown here would be expected to demonstrate more variety in behavior, which could impact the potential benefit of copolymers. At room temperature few of the materials studied here are completely out of glass-rubber transition. Fig. 9 uses the storage moduli from DMA (Fig. 2) to illustrates how these lineshapes should appear for the $(\mathbf{1A12.5\text{-}OMe})_{1-w}$-**r**-$(\mathbf{4A4\text{-}PE})_w$ series at varying temperatures. **1A12.5-OMe** was used as the comb endpoint to avoid the DMA anomalies apparent with **1M12.5-OMe**. The trends in Fig. 9 were generally observed for other series as well. At any given temperature below −50 °C (<T_g) all five samples demonstrate approximately the same modulus and little temperature dependence. At higher temperatures one or more samples is in glass-rubber transition and the trendlines exhibit pronounced curvature as a result of variance in rubbery moduli, transition temperatures, and transition widths. Each of these variables is typically increased by crosslinking. Copolymers present the greatest potential benefit in this high-curvature region. The curvature is gradually reduced as each of the samples enters the rubbery plateau. The residual curvature arises from a non-linear distribution of log E'_r, which is also evident in Fig. 2. The increase in moduli at very high temperatures results from strain hardening.

Given the strong dependence of both conductivity and modulus on $T-T_g$, it is critical to understand the relationship between composition and T_g. However, description of the T_g trends in Table 1 is complex given the simultaneous contributions from end group effects of the PEG sidechains, which are expected to behave as internal plasticizers; covalent crosslinking effects from the di- tri- and tetra-functional monomers; ionic crosslinking effects from the lithium salts, which were previously shown to increase the T_g of the homopolymers [21]; and copolymer effects originating from variations between copolymerized monomers. Each of these effects can impact ion transport behavior of the polymer as well as bulk mechanical properties. For purposes of this study, the data sets as shown in Fig. 3 were fit using the Gordon–Taylor equation [39]:

$$T_g = \frac{(1-w)T_{g1} + kwT_{g2}}{(1-w)+kw} \tag{8}$$

which is an empirical description of the copolymer effect in which T_{g1} and T_{g2} are the respective glass transition temperatures of the comb and crosslinker homopolymers, and k is a constant. The case for $k=1$ reduces equation (8) to the well-known Fox equation [40]. While the Gordon–Taylor equation does not explicitly account for end groups or crosslinking, these effects may be considered to be implicit in the T_g for each comb or crosslinked homopolymer. Of interest here is the smooth transition between homopolymers for each data set, and the increasing non-linearity of the trends with increasing difference between T_{g1} and T_{g2}. The parameter k illustrates this latter trend as shown in Fig. 10. k has been previously correlated to different material parameters, such as the ratio of volume expansion coefficients, and lower values of k are often attributed to less interaction between the polymer constituents [41]. Design of new systems with optimized conductivity or mechanical properties at a given temperature, both dependent on $T-T_g$, may be guided by desired values of T_{g1}, T_{g2} and k.

4.2. Multifunctional properties

Fig. 5 suggests that multicomponent systems may be preferred for simultaneously improving multiple competing properties. In homopolymers, changes in chemistry or bulk architecture do not affect the conductivity-modulus tradeoff since both properties, which have

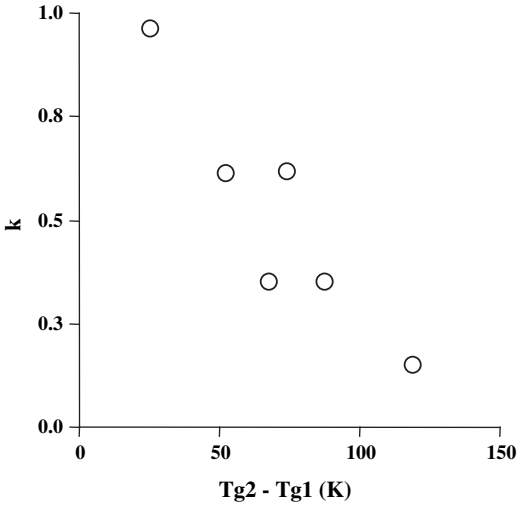

Fig. 10. The Gordon–Taylor fitting parameter, k, vs. the difference in comb and crosslinker T_g for the copolymer systems in Table 1.

competing mechanisms, are significantly reliant on the same species in the polymer (i.e. PEG sidechain or PEG crosslink). In copolymers this interdependence is more decoupled by including both constituents (PEG sidechain and PEG crosslink) to optimize long-range structure as well as long-range ion transport, to yield an improved conductivity-modulus tradeoff. Furthermore, the multifunctional performance is optimized for systems in which the constituents have individually optimized capabilities (e.g. a highly conductive comb plus a high modulus crosslinker). Fig. 5c and d highlight several of the highest performing series within this study.

There are two critical variables that appear to control multifunctionality for the present structural electrolytes: 1) the [homopolymer] endpoints for each system limit the maximum value that may be achieved for individual properties, and 2) the nature of the curve between the endpoints determines how effectively both properties may be simultaneously optimized. Optimization of these two variables should yield materials with improved multifunctionality.

The target for the first variable is to move the endpoints further out from the origin, which is accomplished through changes to the individual constituents (e.g. the homopolymers). This goal may be addressed through the use of different materials than those reported here, particularly through combination of liquid electrolytes and more structural matrices.

The second variable is pertinent to the current research and suggests the desire to generate more of a linear (rather than log–log) interdependence of properties by optimizing the synergistic interaction of the components and/or the microstructure of the material. The curvature of the copolymer trendlines (Fig. 5c and d) discussed in Figs. 7 and 8 is desirable for this purpose. The curvature originates from an inconsistent change in modulus with composition (Figs. 4b and 8) simultaneous to a very consistent change in conductivity (Figs. 4a and 8; equations (5) and (7)). The greatest synergy between properties occurs with lightly crosslinked samples, in which there is a disproportionately large increase in log E'_{rubber} with initial crosslinking (Fig. 2). The consistent response of conductivity to changes in composition, described by equation (5) and apparent as a linear lineshape on a logarithmic axis (Fig. 6), was found for all of the systems studied here regardless of chemistry or architecture. Given that a similar response as described by equation (4) was found for some gel-type electrolytes [33], it is possible that these descriptions may apply to broad spectrum of well-mixed systems. Improvements to multifunctionality *in well-mixed systems* may therefore be more likely to arise from changes in the modulus, particularly with regard to the phase dependence of modulus (Figs. 2 and 9).

One approach to optimization of system multifunctionality is to focus on systems or temperatures in which the phase does not change with composition. Considering the inconsistent temperature dependence of both modulus and conductivity with the physical state of the material, the electrochemical–mechanical relationship should also be strongly dependent on $T-T_g$. Although samples that diverge considerably from the transition region were not thoroughly investigated in this study, compositional changes in copolymers that are isolated to the glassy state are expected to yield a log–linear (conductivity-modulus) tradeoff. Unfortunately, below T_g the conductivity is typically too low to be useful for device purposes, as demonstrated by **2M4.5** ($\sigma \sim 10^{-8}$ S/cm); and in the rubbery region the modulus in suitably conductive materials is often too low to be useful for structural purposes, as demonstrated by **1A12.5-OMe** ($E' \sim 10^{-1}$ MPa) or even **2A30-BPA** ($E' \sim 10^{1}$ MPa). These obstacles may be reduced through development of highly conductive high-T_g electrolytes [42] or through the use of additives that improve rubbery modulus without a comparable detriment to ion transport [14–17].

In the materials presented here, structure originates primarily from high T_g monomers that yield a significant network of rigid crosslinks, and conductivity originates primarily from low T_g monomers that yield a large volume fraction of flexible polyether sidechains. However, these monomers are well-mixed to yield compromised bulk properties. A more useful design approach may be to enable even greater decoupling, perhaps through phase separation and more controlled microstructure, such that a high bulk modulus is retained as well as significant percolation of low T_g (or liquid) conductive regions. In this way the interdependence between properties might be maximized while retaining a useful range for both properties.

5. Conclusion

The objective of this study was to develop polymer electrolytes that optimize simultaneous ion conductivity and mechanical behavior. Previous work investigated a wide variety of homopolymer chemistries and architectures and concluded that these objectives were unlikely to be met in a homogenous system. The current study employed these same materials to formulate solvent-free random copolymers with one monomer selected to promote ion conduction and another monomer selected to promote structural behavior. The ion-conducting monomers generate comb polymers with PEG sidechains that allow for long-range transport of lithium ions. The structural monomers provide for crosslinking by means of including two, three, or four vinyl ester groups on a single monomer. The properties of the resulting copolymers were controlled by varying the type of monomer used from each category as well as the ratio of monomers. For each copolymer system pairing two distinct monomers in variable ratios, the electrochemical-mechanical multifunctional behavior of the copolymer was found to be higher than that of either homopolymer. The relative change in conductivity was found to be consistent as the ratio of monomers was progressed from 100% comb to 0% comb, while the impact on mechanical stiffness was found to decrease over this range. The mechanisms controlling both behaviors were related to polymer mobility and were strongly dependent on the relationship between the measurement temperature and the T_g, particularly as it defined the state of each material.

For the materials in this study, the most useful multifunctional material is achieved not through optimizing a single homogenous material but by rationally combining two or more materials with optimized capabilities. The key points of improving multifunctionality in a material through the use of individual elements, and the disparity with which the individual properties behave as the component composition is changed, may be applied to other mixed systems as future materials are formulated. Controlled segregation of components, particularly evident in block copolymers with immiscible phases, may further optimize the multifunctional effects demonstrated here.

Potential application of these materials is directed towards multifunctional structural batteries, but the wide range of tailorable properties allows them to be emplaced in a variety of dual-function systems. Although the conductivities remain relatively low for traditional battery applications, the synergistic nature of multifunctional structures enables the use of materials with lower that usual properties. Maintaining a sufficiently high modulus, ideally at least 100 MPa, is critical for structural applications. Future efforts will leverage previous work in both traditional composites and solid-state electrolytes, including the use of nano-particle toughners and liquid electrolytes, to optimize system performance in high modulus structural electrolytes. Viscosities of the unreacted systems in this study range from 10 to 1000 cP, which should be low enough to allow for traditional composite processing that requires pressure-induced wetting out of dry fabric preforms. Mixed systems that include solvents are expected to have even lower viscosities. Demonstration

of practical composite processing using novel multifunctional resin-based systems will be presented in later studies.

Acknowledgment

The authors are grateful to Dr. John La Scala, Dr. Rob Carter, Dr. Rob Jensen, Dr. Josh Orlicki, Dr. Joe Lenhart, and Dr. Kang Xu for helpful advice, and to Dr. La Scala for his assistance with the FT-IR experiments. Ms. Watson was supported by the Science and Engineering Apprenticeship Program administered through George Washington University.

References

[1] Wetzel ED. AMPTIAC Quarterly 2004;8(4):91–5.
[2] Thomas JP, Qidwai MA. JOM 2005;57(3):18–24.
[3] Wong EL, Baechle DM, Xu K, Snyder JF, Carter RH, Wetzel ED. Design and processing of structural composite batteries. SAMPE 2007 Symposium and Exhibition. Baltimore, MD, 2007.
[4] Liu P, Sherman E, Jacobsen A. Journal of Power Sources 2009;189:646–50.
[5] Thomas JP, Qidwai MA. Acta Materialia 2004;52(8):2155–64.
[6] Qidwai MA, Baucom JN, Thomas JP, Horner DM. Materials Science Forum 2005;492–493:157–62.
[7] Qidwai MA, Baucom JN, Thomas JP, Horner DM. Multifunctional applications of thin film Li polymer battery cells. Viii. In: Functionally Graded Materials, vol. 492–493. Zurich-Uetikon: Trans Tech Publications Ltd; 2005. p. 157–62.
[8] Snyder JF, Wong EL, Hubbard CW. Journal of the Electrochemical Society 2009;156(3):A215–24.
[9] Snyder JF, Carter RH, Wong EL, Nguyen P-A, Xu K, Ngo EH, et-al. Multifunctional Structural Composite Batteries. 2006 Fall Meeting of the Society for the Advancement of Materials and Process Engineering. Dallas, TX, 2006.
[10] Berthier C, Gorecki W, Minier M, Armand MB, Chabagno JM, Rigaud P. Solid State Ionics 1983;11(1):91–5.
[11] Xu K. Chemical Reviews 2004;104(10):4303–417.
[12] Rupp B, Schmuck M, Balducci A, Winter M, Kern W. European Polymer Journal 2008;44(9):2986–90.
[13] Lenest JF, Gandini A, Cheradame H. British Polymer Journal 1988;20(3):253–68.
[14] Mazor H, Goodnitsky D, Peled E, Wieczorek W, Scrosati B. Journal of Power Sources 2008;178(2):736–43.
[15] Leite ER, Souza FL, Bueno PR, de Lazaro S, Longo E. Chemistry of Materials 2005;17(18):4561–3.
[16] Wen ZY, Wu MM, Itoh T, Kubo M, Lin ZX, Yamamoto O. Solid State Ionics 2002; 148(1–2):185–91.
[17] Zhang XW, Fedkiw PS. Journal of the Electrochemical Society 2005; 152(12):A2413–20.
[18] Trapa PE, Won YY, Mui SC, Olivetti EA, Huang BY, Sadoway DR, et al. Journal of the Electrochemical Society 2005;152(1):A1–5.
[19] Niitani T, Shimada M, Kawamura K, Kanamura K. Journal of Power Sources 2005;146(1–2):386–90.
[20] Jannasch P. Chemistry of Materials 2002;14(6):2718–24.
[21] Snyder JF, Carter RH, Wetzel ED. Chemistry of Materials 2007;19:3793–801.
[22] Liu G, Reinhout M, Mainguy B, Baker GL. Macromolecules 2006;39(14):4726–34.
[23] Adebahr J, Forsyth M, MacFarlane DR, Gavelin P, Jacobsson P. Journal of Materials Chemistry 2003;13(4):814–7.
[24] Erickson MJ, Frech R, Glatzhofer DT. Polymer 2004;45(10):3389–97.
[25] Torquato S, Hyun S, Donev A. Physical Review Letters 2002;89(26):4.
[26] Srobl G. The physics of polymers. 2nd ed. New York: Springer; 1997.
[27] Palmese GR, McCullough RL. Journal of Applied Polymer Science 1992; 46(10):1863–73.
[28] La Scala JJ, Sands JM, Orlicki JA, Robinette EJ, Palmese GR. Polymer 2004; 45(22):7729–37.
[29] Flory PJ. Journal of the American Chemical Society 1941;63(11):3083.
[30] Stockmayer WH. Journal of Chemical Physics 1943;11:45.
[31] Yu XR, Levine SE, Broadbelt LJ. Macromolecules 2008;41(21):8242–51.
[32] Yu Q, Zhou M, Ding YH, Jiang BB, Zhu SP. Polymer 2007;48(24):7058–64.
[33] Yarovoy YK, Wang HP, Wunder SL. Solid State Ionics 1999;118(3–4):301–10.
[34] Adam G, Gibbs JH. Journal of Chemical Physics 1965;43(1):139.
[35] Torquato S, Yeong CLY, Rintoul MD, Milius DL, Aksay IA. Journal of the American Ceramic Society 1999;82(5):1263–8.
[36] O'Brien DJ, Sottos NR, White SR. Experimental Mechanics 2007;47(2):237–49.
[37] Feng XQ, Tian Z, Liu YH, Yu SW. Applied Composite Materials 2004;11(1):33–55.
[38] Tilbrook MT, Moon R, Hoffman M. Materials Science and Engineering A-Structural Materials Properties Microstructure and Processing 2005; 393(1-2):170–8.
[39] Gordon M, Taylor JS. Journal of Applied Chemistry 1952;2(9):493–500.
[40] Fox TG. Bulletin of the American Physical Society 1956;1:123.
[41] Mohamed AA, Xu JY. Journal of Applied Polymer Science 2007;106(1):214–9.
[42] Wei XY, Shriver DF. Chemistry of Materials 1998;10(9):2307.